BMC Neuroscience

Research article

Ultrastructure of acetylcholine receptor aggregates parallels mechanisms of aggregation

Dennis D Kunkel, Lara K Lee and Jes Stollberg*

Address: Békésy Laboratory of Neurobiology, University of Hawaii at Manoa Honolulu, HI 96822, USA

E-mail: Dennis D Kunkel - kunkel@hawail.rr.com; Lara K Lee - laralee@hawaii.edu; Jes Stollberg* - jesse@pbrc.hawaii.edu
*Corresponding author

Published: 10 December 2001

BMC Neuroscience 2001, **2**:19

Received: 9 August 2001
Accepted: 10 December 2001

This article is available from: http://www.biomedcentral.com/1471-2202/2/19

Abstract

Background: Acetylcholine receptors become aggregated at the developing neuromuscular synapse shortly after contact by a motorneuron in one of the earliest manifestations of synaptic development. While a major physiological signal for receptor aggregation (agrin) is known, the mechanism(s) by which muscle cells respond to this and other stimuli have yet to be worked out in detail. The question of mechanism is addressed in the present study via a quantitative examination of ultrastructural receptor arrangement within aggregates.

Results: In receptor rich cell membranes resulting from stimulation by agrin or laminin, or in control membrane showing spontaneous receptor aggregation, receptors were found to be closer to neighboring receptors than would be expected at random. This indicates that aggregation proceeds heterogeneously: nanoaggregates, too small for detection in the light microscope, underlie developing microaggregates of receptors in all three cases. In contrast, the structural arrangement of receptors within nanoaggregates was found to depend on the aggregation stimulus. In laminin induced nanoaggregates receptors were found to be arranged in an unstructured manner, in contrast to the hexagonal array of about 10 nm spacing found for agrin induced nanoaggregates. Spontaneous aggregates displayed an intermediate amount of order, and this was found to be due to two distinct population of nanoaggregates.

Conclusions: The observations support earlier studies indicating that mechanisms by which agrin and laminin-1 induced receptor aggregates form are distinct and, for the first time, relate mechanisms underlying spontaneous aggregate formation to aggregate structure.

Background

One of the first observable changes at a developing neuromuscular synapse is the aggregation of nicotinic acetylcholine receptors (AChRs) in the postsynaptic membrane. This aggregation can be detected within several hours of stimulation by a nerve terminal or by alternative stimuli, and is crucial to the function of the mature synapse in that it ensures both speed and reliability of signal transduction. Extensive studies in varied experimental systems have identified specific intra-cellular [1–5] and extra-cellular [6–11] components which appear to be involved in the formation and maturation of AChR aggregates.

In addition to a contacting nerve terminal, receptor aggregation can be induced by several experimental stimuli

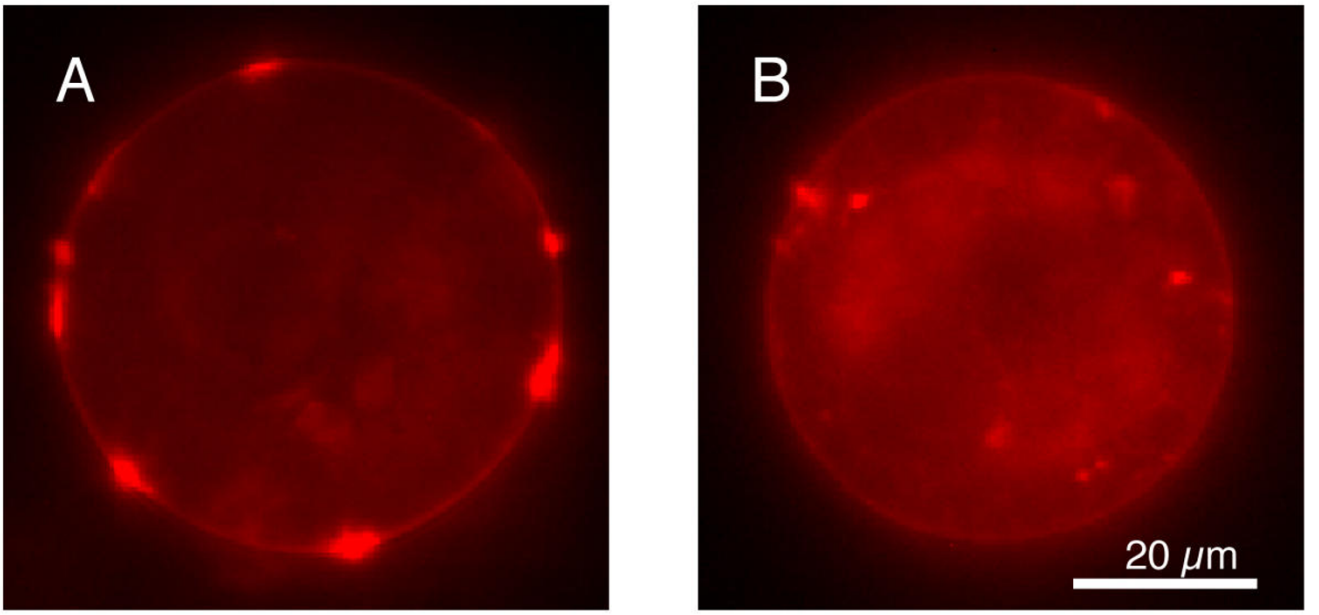

Figure 1
Fluorescent micrographs of *Xenopus* muscle cells stimulated with laminin-1 (A) and under control conditions (B). Cells were labeled for AChRs with rhodamine α-Bungarotoxin. Sources of light internal to the cell membrane correspond to autofluorescence and should be ignored. Note the increase in the size and number of aggregates found following stimulation with laminin-1.

including agrin [11–13], electric fields [14–18], polystyrene beads [19,20], culture substratum [21,22], and high calcium or neuraminidase [23–26]. Among these agrin is the only one for which a strong argument of physiological relevance can be advanced. Published accounts have demonstrated that the neuromuscular junction does not develop in agrin deficient mutant mice[27], in strong support of "the agrin hypothesis"[28].

More recently a member of the laminin family, laminin-1, has been shown to induce AChR aggregation. Interestingly, this induction appears to be independent of the mechanism(s) by which agrin acts based on an additive dose response relationship, the lack of requirement for MuSK, and the lack of tyrosine-phosphorylation of receptors during aggregation [29–31]. Note that in this context "independent" simply means that there is at least some difference in the two sequences of events besides the signaling event, and (from the dose response data) that the two sequences do not share a rate limiting step. The existence of independent pathways is important because many studies over the past decades have implicitly assumed that receptor aggregation, whether spontaneous or induced by various stimuli, constitutes a single phenomenon carried out by a common mechanism.

To further address the extent to which commonality of mechanism exists in differentially induced receptor aggregates we have compared the ultra-structural arrangement of receptors within spontaneous and agrin or laminin-1 induced aggregates. We previously demonstrated that agrin induced receptor aggregates are aligned on a hexagonal grid of ca. 9.9 ± 0.5 nm spacing [32–34]. We show now that laminin-1 induced receptor aggregates do not exhibit this regularity in ultrastructure, while spontaneous receptor aggregates display heterogeneous characteristics, with some aggregates showing regular spacing while others do not.

Results

Laminin-1 clearly induces AChR aggregation over and above that found spontaneously in control cells (Figure 1). Using software designed to quantify aggregate number, size, and position similar to that reported previously[35], we have determined that there are significant increases in both number and size of receptor aggregates following treatment with laminin-1 (e.g. aggregates per cell = 6.4 ± .23 vs. 4.9 ± .26 for control, Student T $p < .0001$[36]). This finding parallels reports in mouse muscle cells[29,30], but is in contrast to one report from *Xenopus*[31].

At the level of scanning electron microscopy, membrane regions rich in AChRs (whether spontaneous or induced by agrin or laminin) show receptor distributions which appear decidedly non-random (Figure 2). That is, numerous "nanoaggregates" – very dense nanometer scale particle clusters – are seen which give an appearance markedly different from what is seen, for example, in plots of points selected at random. This heterogeneous, nanoaggregate rich visual impression is confirmed by quantitative analysis of the nearest neighbor distances (Figure 3). In both laminin induced and control AChR aggregates there are far more small (10–50 nm) distances found than would be expected in truly random distributions (Figure 3A and 3B, dashed curve; see Materials and methods for theoretical distribution). This means that many receptors are closer to each other than predicted by a random distribution, exactly as would be expected by the formation of nanoaggregates. The same theoretical random particle distribution function can be better fit to the data by artificially increasing the density many fold (solid curves). These are still statistically inconsistent with the data of Figure 3, A and 3B, in part because the predictive equation assumes a sharp cutoff at the hindrance distance (Materials and methods) while the data clearly show a more gradually decreasing probability as a (somewhat smaller) hindrance distance is approached.

With respect to structure within aggregates, the arrows in these figures indicate the positions at which agrin induced receptor aggregates were found to peak, which indicated that receptors were arranged in a hexagonal array with a spacing of approximately 9.9 nm[33,34]. It can be seen that these peaks are not present in laminin-1 induced aggregates (A), but may be weakly present in the spontaneous receptor aggregates (B). To examine whether these small peaks in the 20–40 nm range are significant, the distributions were fit to quadratics and tested statistically against them. This is not to suggest a quadratic form for the distribution, but rather to test whether that region of a distribution is consistent with a smoothly decreasing function. It was determined that laminin-1 induced aggregate structure is in fact consistent with this, but that spontaneous aggregate structure is not (Figure 3, legend). Thus it appears that at least some of the peaks seen in spontaneous aggregate nearest neighbor distances are significant.

To probe further into aggregate structure software was designed to detect nanoaggregates (Materials and methods). Figure 4 shows a plot of a scanning electron micrograph montage, revealing the overall ultrastructural arrangement of AChRs. The colors illustrate the aggregate detection algorithm and confirm that its function is consistent with what the human eye detects as nanoaggregates Two representative nanoaggregates are shown in Figure 5, which also illustrates the measurements applied to them. These are size (number of gold particles), density, and two measures of spherical vs. oblong shape: the normalized area/perimeter ratio, and the diameter ratio (Materials and methods). Table 1 shows the mean and standard error of these measures applied to laminin induced, spontaneous, and agrin induced receptor aggregates. No significant differences are seen in any of these measures between laminin induced and spontaneous aggregates. However compared to either of these, agrin induced aggregates are significantly larger and *less* dense in terms of gold particle distribution (Student T $p < .001$). Although it is at first glance counter-intuitive, this decrease in particle density (agrin induced aggregates) is best interpreted as an *increase* in receptor density (see Discussion). Table 2 shows the correlation between these measures when all three experimental treatments are pooled (n = 292).

There appears to be a modest negative correlation between size and density. This means that larger aggregates tend to have a lower density of gold particles, in

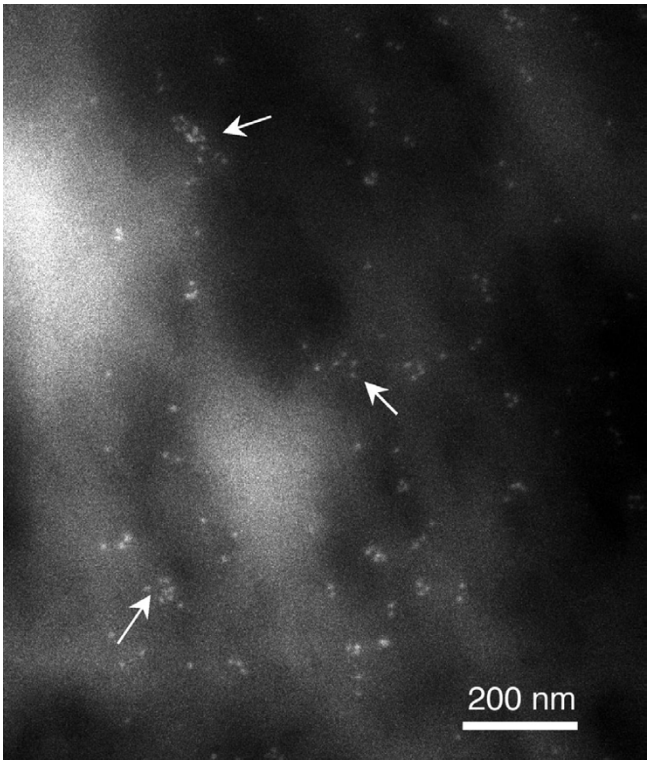

Figure 2
Scanning electron micrograph of *Xenopus* muscle cell membrane stimulated with laminin-1 and immuno-gold labeled for AChRs. The particles appear to be arranged into nanoaggregates (arrows) suggesting a non-random distribution.

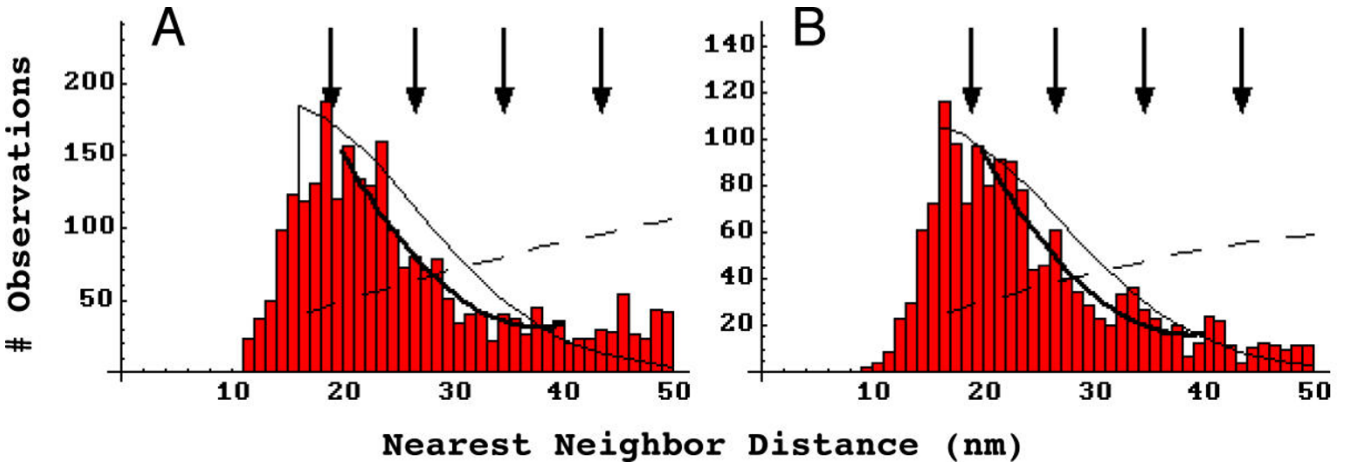

Figure 3
Frequency histograms of experimental nearest neighbor distances. A, laminin-1 induced receptor aggregates (n = 2581, n-reduced = 1468). B, spontaneous receptor aggregates (n = 1527, n-reduced = 905). Arrows, prominent in peaks in agrin-induced receptor aggregates, do not characterize laminin-induced aggregates (A) but may be present in spontaneous aggregates (B). A compared to B, Pearson χ^2 p < .0001. Dashed curves, the probability density functions for randomly distributed particles with a hindrance of 16 nm at the respective densities found. A or B compared to data, Pearson $\chi^2 < 10^{-10}$. Solid curves – the same functions with the density terms artificially elevated to best approximate the distributions in the range 20 to 40 nm. A or B compared to data, Pearson χ^2 p < 10^{-10}. Heavy solid curves, best fit quadratics over the range 20 to 40 nm. A, 300.75 - 14.67 x + 0.19 x^2, Pearson χ^2 p > 0.22. B, 196.41 - 9.45 x + 0.12 x^2, Pearson χ^2 p < 0.02.

agreement with the finding that agrin induced nanoaggregates are both larger and less dense than those of laminin induced or spontaneous nanoaggregates Although there may be a small negative correlation between density and the area/perimeter ratio this would at best account for only 15% of the variation seen in these measurements, and seems to be contra-indicated by the much smaller correlation between density and the diameter ratio. This latter ratio and the area/perimeter ratio are highly correlated, confirming that they measure approximately the same shape attribute along the linear-to-circular dimension (Materials and methods).

The apparently weak regular structure seen in spontaneous receptor aggregates suggests two possibilities. First, it could be that these nanoaggregates are homogeneous with respect to structure, and they all display an underlying hexagonal structure which is partially masked by "misplaced" receptors within these aggregates. At the other extreme, it could be that there are two populations of spontaneous nanoaggregates, one of which shows significant hexagonal structure while the other does not. Despite the similarities in the means and variances of the 4 measures for laminin induced and spontaneous nanoaggregates, an examination of the underlying frequency histograms revealed one suggestive difference in this regard. Figure 6 shows the frequency histograms for density in laminin-1 induced (A) and spontaneous (B) nanoaggregates The former appears to be a simple, skewed distribution, but the latter appears to be bimodal, thereby suggesting that there may indeed be two underlying populations.

Because of this, and the difference in particle density seen in agrin induced nanoaggregates, we examined the nearest neighbor distances distribution for the two populations – one above and one below the density median (Figure 7). In Figure 7A it is seen that the high density fraction of spontaneous nanoaggregates shows very little in the way of regular structure. On the other hand Figure 7B shows an improved match of the low density fraction to the predicted peaks (arrows) which represent a hexagonal array of 9.9 nm spacing. In fact this low density population is not significantly different from the modeled distribution based on the geometry and spacing assumptions previously presented (Figure 7, legend)[33,34]. Moreover this difference in density and orderliness cannot be attributed to subtle experimental variations from preparation to preparation: of 21 control images containing more than one nanoaggregate, 18 contained nanoaggregates both above and below the median density (see Discussion). Thus the latter hypothesis presented above appears to be the valid one: spontaneous receptor aggregates are heterogeneous, with some showing well ordered structure and others none at all.

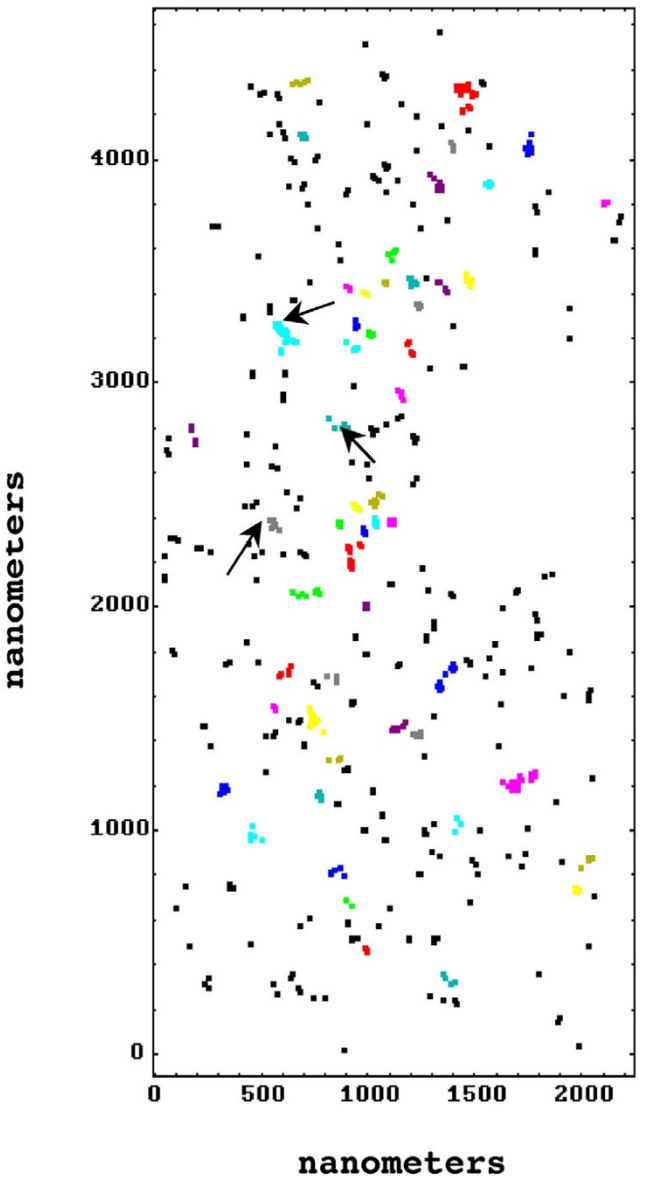

Figure 4
Digital montage of seven overlapping micrographs showing gold label locations in a cell stimulated with laminin-1. Arrows, positions of nanoaggregates marked in Figure 2. The different colors represent the distinct nanoaggregates identified by software (black points are not members of any nanoaggregate).

Discussion

This work was undertaken with the expectation that the ultrastructure of AChR aggregates – whether spontaneous or induced by laminin-1 – would either be ordered like those of agrin induced aggregates, or unordered. As often transpires the experimental results lead in a direction that is both more complicated and more interesting. In interpreting our results it is useful to keep clearly in mind the different spatial scales of observation. Accordingly we have used the term "nanoaggregates" to denote phenomena at the nanometer scale of resolution, as distinguished from the commonly used "microaggregates" which indicates aggregation observations at the micron scale.

Laminin-1 clearly induces microaggregation of receptors after 24 hours in our culture system (Figure 1). This finding conflicts with a recent report based on a similar approach[31], although the differences in the system may be significant. In the cited work embryonic *Xenopus* myocytes were cultured onto a rat tail collagen substrates, which promotes cell adhesion and a flattening out of the cells, and incubated at a laminin concentration of up to 6 nM. The authors report that control (unstimulated) cultures under these conditions typically display 1–2 AChR "megaclusters" (> 40 μm) on the ventral surface. In our system the myocytes are plated onto clean glass coverslips, typically do not flatten out on the substrate, and display only small microaggregates, if any, in controls (e.g. Figure 1B). Thus the induction of receptor aggregates by laminin-1 may be either statistically or physiologically masked by the presence of pre-existing large aggregates in the earlier work. Alternatively it may be that their culture system would have shown receptor aggregation at the laminin concentration used in the present study (30 nm).

Receptor aggregates (spontaneous or induced by laminin-1) are clearly not randomly distributed on a nanometer scale. Instead, and like agrin induced aggregates, they form discrete nanoaggregates (Figures 2 & 3) in a manner termed heterogeneous aggregation [32–34]. The alternative, completely consistent with all light microscopic evidence, would be a spatially uniform and random distribution of receptors which are simply at a higher density than in membrane not displaying aggregation on the micron scale (homogeneous aggregation).

Notwithstanding this global nonrandom distribution of receptors, laminin induced receptor aggregates do not show evidence of the ordered structure previously found in agrin induced receptor aggregates (Figure 3). Rather than a nearest neighbor distance profile showing preferred distances consistent with a hexagonal spacing of receptors, the nearest neighbor distances within laminin induced aggregates are consistent with an unstructured distribution. This difference in ultrastructure parallels recent reports suggesting that agrin and laminin induce receptor aggregates via different mechanisms [29–31], and confirms our working hypothesis that detailed analysis of aggregate ultrastructure can provide important clues to aggregation mechanisms.

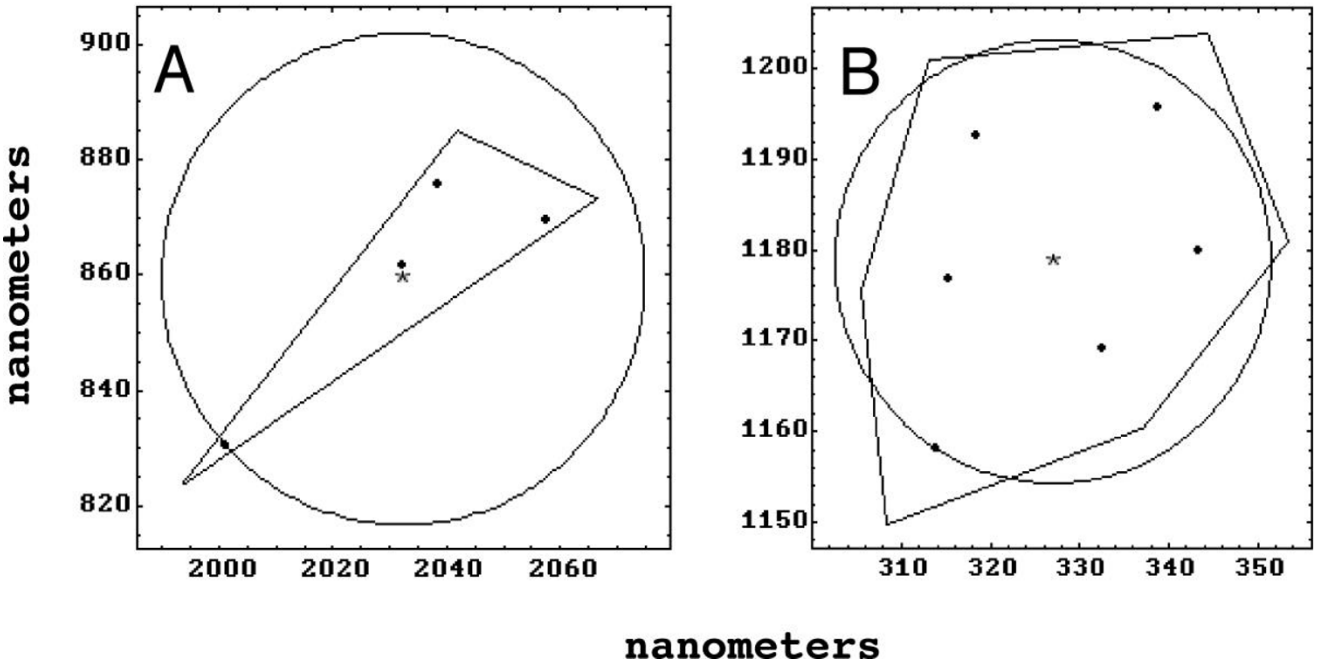

Figure 5
Examples of gold particle nanoaggregates identified by software. The polygons represent the defined perimeter (Materials and methods), the asterisks the center of mass, and the circles are the smallest centered on the asterisks that encompass all points within the nanoaggregates. A, size = 4 gold particles, density = 3876 particles/μm2, normalized area/perimeter ratio = 0.35, diameter ratio = 0.43. B, size = 6 particles, density = 3333/μm2, area/perimeter ratio = 0.83, diameter ratio = 0.98.

Table 1:

Treatment	Laminin	Spontaneous	Agrin
Measurement			
Size	5.09 ± 0.17	5.12 ± 0.16	7.11 ± 0.46
Density	2817 ± 98	2995.6 ± 115	1864 ± 99
Area/Perimeter	0.57 ± 0.01	0.57 ± 0.02	0.60 ± 0.02
Diameter Ratio	0.69 ± 0.02	0.68 ± 0.02	0.66 ± 0.02
(N)	(105)	(99)	(88)

Table 2:

Measurement	Size	Density	Area/ Perimeter	Diameter Ratio
Size	-	-0.48	0.27	-0.040
Density	-	-	-0.39	-0.006
Area/Perimeter	-	-	-	0.86

With regard to spontaneous receptor aggregation, our findings indicate that the weak display of structure results not from uniformly weak nanoaggregate ordering, but from two classes of aggregates. Those characterized by a lower density of gold particle label have an ultrastructural arrangement like that of agrin induced receptor aggregates (hexagonal array, ~10 nm spacing), while those displaying a higher density are relatively unstructured and are in this respect like the nanoaggregates induced by laminin-1 (Figure 7).

Could the presence or absence of orderly nanoaggregate structure be accounted for by subtle differences in culture or fixation technique from experiment to experiment, or over time? If this were true we would have expected similar outcomes from laminin induced and spontaneous aggregates, which were not observed. Moreover this hypothesis predicts that, in the case of our spontaneous aggregate experiments, low and high density nanoaggregates would be found on mutually exclusive sets of slides. Instead we found that individual slides, and indeed individual cell images, displayed both low and high density nanoaggregates. Therefore we conclude that differences in structure cannot be attributed to unintended variations in treatment, and are instead due to

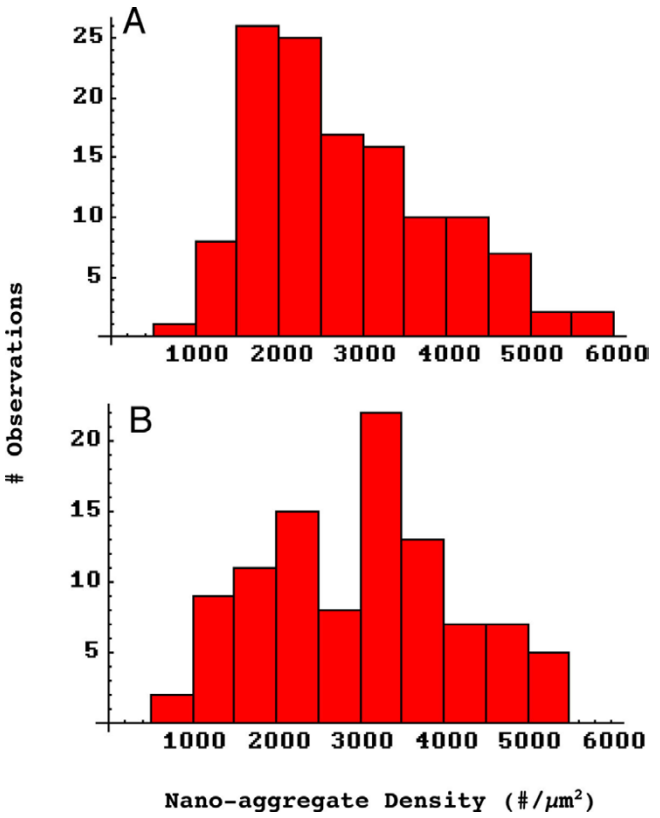

Figure 6
Frequency histograms of nanoaggregate density. A, laminin-1 induced receptor aggregates (n = 124). B, spontaneous receptor aggregates n = 99). The latter distribution appears to be bimodal, suggesting that there may be two populations of spontaneous aggregates. A compared to B, Pearson χ^2 p < .001.

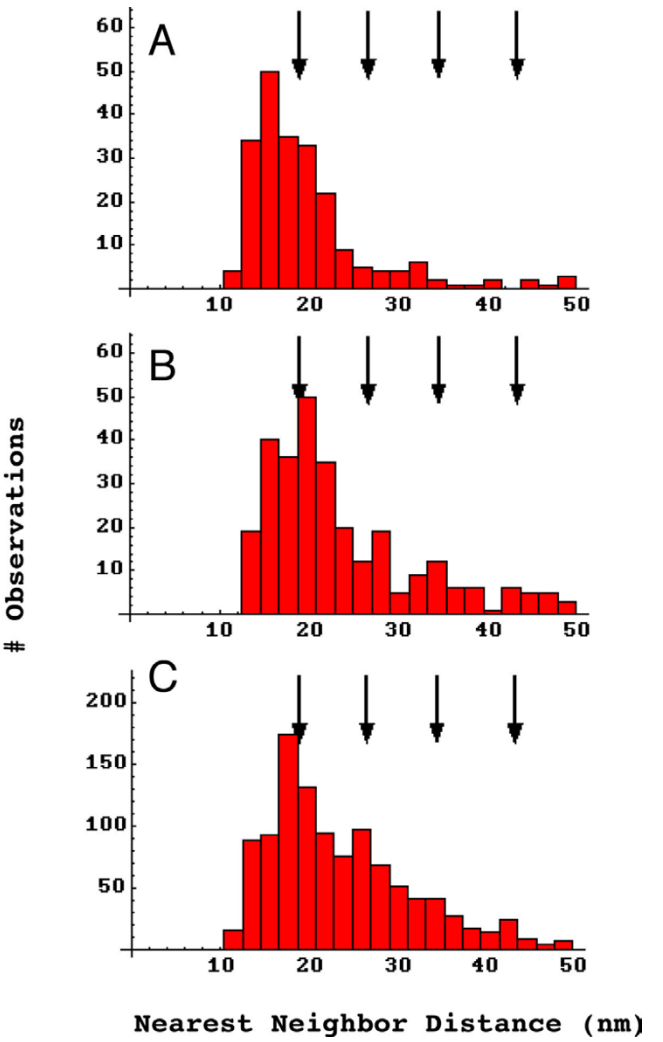

Figure 7
Frequency histograms of experimental and simulated nearest neighbor distances. A, high density receptor aggregates (n = 218, n-reduced = 146). B, low density receptor aggregates (n = 289, n-reduced = 178). C, simulation of nearest neighbor distances assuming a hexagonal array of receptors with a spacing of 9.9 nm. Arrows, prominent in peaks in agrin-induced receptor aggregates, do not characterize high density aggregates (A) but appear to be represented in low density aggregates (B). A vs. C, Pearson $\chi^2 < 10^{-10}$. B vs. C, Pearson $\chi^2 > 0.13$.

real differences in the physiological events resulting in aggregation.

At first glance it may seem surprising that it is the *lower* density nanoaggregates – as measured by gold particle density – which present a more ordered ultrastructural arrangement. For that matter, since the ordered nanoaggregates are packed at nearly the maximal possible density[33], how can other nanoaggregates have a significantly higher density (Table 1)? The resolution of this apparent paradox resides in the distinction between differences in gold particle density (which are observed), and the underlying receptor density (which must be inferred). As previously reported, the labeling paradigm used here precludes the labeling of adjacent receptors in hexagonally arranged nanoaggregates[33]. This means that gold particle density can actually be increased in lower receptor density, unordered aggregates (Figure 8). In fact the maximum possible increase in receptor density from a 9.9 nm hexagonal array, assuming a receptor diameter of 8.5 nm, is about 33% – significantly less than that seen for the gold particle density differences in Table 1. Thus the only interpretation that can be given to our findings is that the receptor density within nanoaggregates is actually higher in those induced by agrin than those induced by laminin. Furthermore it is the higher receptor density (lower particle density) spontaneous aggregates which, like agrin induced aggregates, show a regularly ordered structure.

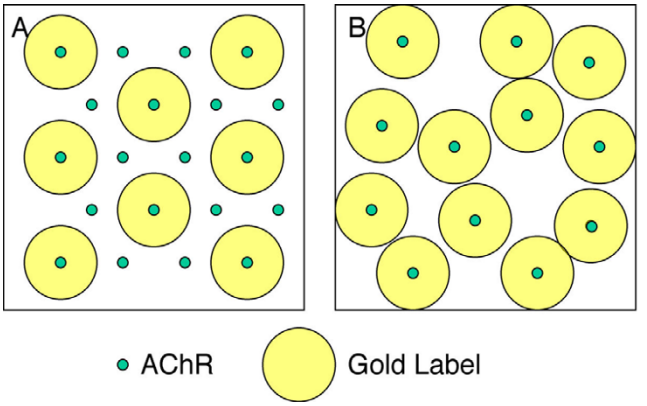

Figure 8
Schematic of gold label locations in hexagonal and random nanoaggregates. The size of the gold label symbol represents the known steric hindrance of the labeling paradigm, which includes two antibodies as well as the gold particle itself. A, 20 AChRs lie on a hexagonal grid, which can be labeled by at most 8 gold particles because of steric hindrance. B, only 12 AChRs are present in this randomly arrayed nanoaggregate, but the density of gold particles is higher (12 particles per unit area) than in A. For purposes of illustration this figure assumes that every receptor which can be is labeled, however the argument holds at lower binding efficiencies as well.

As discussed previously there is growing evidence for at least two mechanistic pathways of AChR aggregation. One of these is characteristic of agrin, which involves the phosphorylation of MuSK and the receptor as well as the colocalization of α-Dystroglycan, and in our studies produces a regularly ordered structure. The second is exemplified by the stimulus of laminin-1 which does not involve receptor or MuSK phosphorylation or α-Dystroglycan colocalization [29–31], and does not result in an ordered structure within nanoaggregates. We will denote the former as the agrin pathway without caveat, as agrin has clearly been shown to play an important physiological role in receptor aggregation and synapse formation *in vivo*. The latter we will term the laminin pathway for convenience, but with an understanding that the term may be misleading as the physiological role for laminin has not been established. In particular it has not been determined whether the role of laminin-1 is instructive or simply permissive with respect to receptor aggregation.

Into the agrin pathway we can add neuraminidase and elevated calcium based on the biochemical criteria[24], and competition studies suggest that electric fields also induce receptor aggregation via the agrin pathway[35,37]. Other stimuli may later be added to either the agrin or laminin pathway, and one prediction from the present work is that classification based on biochemical mechanism and ultrastructural arrangement will be found to be mutually consistent.

This brings us to a consideration of the dichotomous nature of spontaneous aggregates with respect to structure, and presumably with respect to the mechanism of aggregate formation. What is to be made of the existence of these two classes of nanoaggregates? The most likely interpretation is that low level aggregation occurs spontaneously (laminin pathway), and that in a fraction of these events the maturation of nanoaggregates then transpires, resulting in ordered structure (agrin pathway). The size of this fraction is presumed to be smaller than that actually detected because the established aggregates are expected to have a longer lifetime in the plasma membrane. An alternative interpretation holds that spontaneous receptor aggregation proceeds along the agrin pathway, producing ordered aggregate structure, and that absent some confirming signal these decay into unstructured aggregates which are then detected as part of the population. If the biochemical and structural data do indeed coincide, this would also involve the removal of colocalized α-Dystroglycan and the dephosphorylation of MuSK in the nanoaggregates environment. In point of fact the unordered aggregates detected in our experiments could result from both immature and senescent aggregates, although the latter would be expected to have very short lifetimes and therefore be difficult to detect.

Finally our present work leads us to speculate, pending further results, that the present classification of aggregation pathways may also map onto more functional concepts, such as "preliminary induction" (the laminin pathway) and "maturation and stabilization" (the agrin pathway; see also [38]). This tentative classification is based principally on the observation that agrin, in the absence of laminin, gives rise to structured receptor nanoaggregates, so that it seems in a sense to be a complete stimulus, while laminin-1 appears to take receptors only part of the way toward mature and stabile receptor aggregates, based on structure and additional criteria already discussed. Others have hypothesized alternatively that laminin plays a role in aggregate stabilization, based largely on the difference in mechanism and on the longer response time for laminin as opposed to agrin[30]. These opposing possibilities are equally speculative, and their sorting out will require further experimental examination.

Conclusions

1. Receptor rich cell membranes show non-random distributions of receptors whether they are spontaneous or stimulated via agrin or laminin. This confirms the visual impression that receptors are organized into very dense

nanoaggregates which are too small to be resolved at the level of light microscopy.

2. Despite the forgoing similarity, the ultrastructural arrangement of receptors within nanoaggregates depends on their genesis. Agrin induced receptor aggregates lie on a hexagonal array with a spacing of ca. 10 nm, while laminin-1 induced microaggregates display an irregular or unstructured configuration.

3. Spontaneous nanoaggregates, taken as a whole, are found to be intermediate in degree of order, evidencing more ordered structure than laminin-1 induced aggregates, but less than agrin induced aggregates. Further analysis shows that this is the result of two populations of nanoaggregates in unstimulated cells; a) a population with high receptor density and orderly structure, and b) a population with lower receptor density and disorderly structure.

4. Differences in the ultrastructural arrangement of acetylcholine receptors within aggregates parallel the different geneses of aggregation, and provide important clues respecting the mechanisms of aggregation.

Materials and Methods

Cell culture

Embryonic *Xenopus laevis* muscle cell cultures were prepared according to previously described methods [15]. In brief somites were dissected from stage 17–19 embryos in collagenase/Steinberg's solution, dissociated in $Ca^{+2}Mg^{+2}$ free Steinberg's, and cultured on sterile round (12 mm) coverslips with a small drop of medium (85% Steinberg's solution, 10% Leibovitz's L-15 medium, 5% fetal bovine serum, 50 μg/ml Gentamycin, pH 7.8). Cultures were maintained in plastic petri dishes within a humidified darkened chamber (23°C) for 24 hours before experimentation.

Immunolabeling and high resolution preparation

Muscle cell cultures were treated for 24 hours with laminin-1 (30 nM, Sigma L2020), 2 hours with 10% Agrin(4,8)[33], or left in medium only (controls), rinsed briefly and fixed in 1% paraformaldehyde / 0.02% glutaraldehyde containing 150 mM sucrose, 10 mM $CaCl_2$, and 10 mM $MgCl_2$ in deionized water for 25 minutes (22°C). After rinsing in medium diluted 1:1 with 280 mM sucrose and 0.08% NaN_3 in water, cells were labeled with 600 nM α-Bungarotoxin-biotin (Molecular Probes, Eugene, OR) followed by immunocytochemical detection (mouse monoclonal anti-biotin, 1:500; goat anti-mouse IgG-12 nm gold, 1:10; Jackson ImmunoResearch Labs, West Grove, PA). Controls used were: 1) α-Bungarotoxin only, 2) no α-Bungarotoxin, 3) no anti-biotin and 4) no goat anti-mouse IgG-gold. No gold was seen in controls 1 and 4, and only an occasional gold particles were observed in controls 2 and 3 (0.16 gold particles/μm^2 on average). In some experiments cells were labeled in the first instance with both rhodamine and biotinylated α-Bungarotoxin, followed by the secondary steps outlined above. This permitted viewing and mapping of AChR aggregates for selected study at the SEM level.

In order to limit cell shrinkage and membrane distortion in these cells a four-step postfixation (30 minutes per step) was employed. 1) 1% paraformaldehyde and 0.02% glutaraldehyde containing 0.15 M sucrose; 2) 1% paraformaldehyde / 0.2% glutaraldehyde containing 0.15 M sucrose; 3) 1% paraformaldehyde / 1% glutaraldehyde containing 0.15 M sucrose; 4) 1% paraformaldehyde / 2% glutaraldehyde containing 0.19 M sucrose. Cells were rinsed sequentially in 0.2 M and 0.1 M sodium cacodylate buffer (pH 7.4) and postfixed in 1% OsO_4 in 0.1 M sodium cacodylate for 30 minutes. After rinsing in the same buffer cells were dehydrated in a 10% increasing graded ethanol series (5 mins each) to 100% and critical point dried in a Tousimis Autosamdri Critical Point Dryer. Critical point dried coverslips were mounted on stubs and sputter coated with a very light layer of gold/palladium at 10 mAmp for 5–7 seconds using a Hummer II Sputter Coater.

Data collection and quantitative analysis

Coverslips were examined with an Hitachi S-800 Field Emission scanning electron microscope using a Robinson backscattered detector. SEM working parameters included: accelerating voltage = 15 kv; specimen stage = zero tilt; working distance = 6 mm. Cell membrane areas were sampled as follows: 1) Cells were observed at a magnification of 5,000 with both secondary electron imaging and backscattered electron imaging (BEI). Cells were selected for minimal membrane shrinkage and BEI background noise. 2) These cells were then scanned briefly at 100,000 magnification to determine if cell membrane morphology was consistent and whether gold label was present. Subsequently regions of membrane rich in gold-labeled receptors were scanned as backscattered digital micrographs. For the digital montage figure a series of overlapping images were taken and subsequently merged digitally. Backscattered electron images taken from laminin-1 treated and control cells were imported into Mathematica® for quantitative analysis. Gold particles were located either by eye and computer mouse or by software using image convolution for automated detection (Appendix). Comparison of the two methods showed no significant differences with respect to the reported observations. Scale bar lengths were marked by hand to convert {x,y} coordinates into a nanometer scale. The estimated error from digitization and marking was less than 2 nm.

The coordinates were used to generate frequency histograms of nearest neighbor distances(see [32–34]). These were compared to data reported previously for agrin induced receptor aggregates and to simulations found to account for these earlier observations, as well as the predicted probability density function for randomly distributed particles:

$$p(D) = \begin{cases} D < h, & 0 \\ D \geq h, & \pi\rho D \bullet e^{\pi\rho\left(h^2 - D^2\right)} \end{cases}$$

where ρ is the density, D is the nearest neighbor distance, and h is the spatial hindrance (the closest two particles can approach).

The analysis was also used to identify nanoaggregates, defined as a set of 4 or more particles which can be connected by chords • 50 nm. Four measurements were performed and compared with respect to nanoaggregates: size, density, area/perimeter ratio, and diameter ratio. Aggregate size is defined as the number of gold particles present. Aggregate density is the number of gold particles (not receptors) per μm^2. This calculation requires a definition of the perimeter – a boundary lying somewhere between the points included in the nanoaggregates and those excluded. A margin of 10 nm from included receptors was arbitrarily chosen.(see Figure 5). Because of the necessarily arbitrary rendering of the perimeter, the density measurements (and the area/perimeter ratio described below) are useful only for comparisons within experiments described here. The next two measurements were designed to characterize the shape of nanoaggregates in a dimension indicating more linear (tending to 0) or more circular (tending to1). They were both employed in the thought that they depend on different assumptions about geometry, and might show different results. The normalized area/perimeter ratio was calculated from the perimeter (P) and its encompassed area (A) by the equation

$$4\pi A / P.$$

The diameter ratio was calculated as the diameter of a circle which could just contain the number of particles at the measured density (rearranged to minimize the perimeter) divided by the diameter of the smallest circle, centered at the center of mass, which just contains the particles in their actual configuration. This is calculated as

$$\frac{2\sqrt{A/\pi}}{d_{\max}},$$

where A is the observed area and d_{max} is the maximal diameter of the aggregate. Both of these measures return a value of 1.0 for perfectly spherical aggregates and approach 0.0 as the aggregates become increasingly linear.

The significance of the differences between distributions was determined by the Pearson χ^2 statistic. Because of inherent redundancies in nearest neighbor distributions, the data (and simulations) were reduced prior to comparison (see Appendix).

Acknowledgements

This research was supported by National Science Foundation Grant IBN97-24035, and American Heart Association – Hawaii Affiliate Grant HIGS-17-95. We gratefully acknowledge technical support from Ms. Tina Carvalho, Dr. Marilyn Dunlap and Dr. Brad Jones.

References

1. Campanelli JT, Roberds SL, Campbell KP, Scheller RH: **A role for dystrophin-associated glycoproteins and utrophin in agrin-induced AChR clustering.** *Cell* 1994, **77**:663-674
2. Bloch RJ, Randall WR: **Synapse development: Up the junction.** *Curr Biol* 1994, **4**:936-938
3. Luther PW, Samuelsson SJ, Pumplin DW, Bloch RJ: **Clustered acetylcholine receptors have two levels of organization in Xenopus muscle cells.** *Cell Motil Cytoskeleton* 1994, **28**:179-193
4. Rochlin MW, Peng BH: **Localization of intracellular proteins at acetylcholine receptor clusters induced by electric fields in Xenopus muscle cells.** *J Cell Sci* 1989, **94**:73-83
5. Pumplin DW: **Acetylcholine receptor clusters of rat myotubes have at least three domains with distinctive cytoskeletal and membranous components.** *J Cell Biol* 1989, **109**:739-753
6. Patthy L, Nikolics K: **Functions of agrin and agrin-related proteins.** *Trends Neurosci* 1993, **16**:76-81
7. Nastuk MA, Fallon JR: **Agrin and the molecular choreography of synapse formation.** *Trends Neurosci* 1993, **16**:72-76
8. Bayne EK, Anderson MJ, Fambrough DM: **Extracellular matrix organization in developing muscle: correlation with acetylcholine receptor aggregates.** *J Cell Biol* 1984, **99**:1486-1501
9. Wallace BG: **Agrin-induced specializations contain cytoplasmic, membrane, and extracellular matrix-associated components of the postsynaptic apparatus.** *J Neurosci* 1989, **9**:1294-1302
10. Bloch RJ, Pumplin DW: **Molecular events in synaptogenesis: nerve-muscle adhesion and postsynaptic differentiation.** *Am J Physiol* 1988, **254**:C345-364
11. Godfrey EW, Dietz ME, Morstad AL, Wallskog PA, Yorde DE: **Acetylcholine receptor-aggregating proteins are associated with the extracellular matrix of many tissues in Torpedo.** *J Cell Biol* 1988, **106**:1263-1272
12. Nitkin RM, Smith MA, Magill C, Fallon JR, Yao YM, Wallace BG, McMahan UJ: **Identification of agrin, a synaptic organizing protein from Torpedo electric organ.** *J Cell Biol* 1987, **105**:2471-2478
13. Wallace BG: **Aggregating factor from Torpedo electric organ induces patches containing acetylcholine receptors, acetylcholinesterase, and butyrylcholinesterase on cultured myotubes.** *J Cell Biol* 1986, **102**:783-794
14. Orida N, Poo MM: **Electrophoretic movement and localisation of acetylcholine receptors in the embryonic muscle cell membrane.** *Nature* 1978, **275**:31-35
15. Stollberg J, Fraser SE: **Acetylcholine receptors and concanavalin A-binding sites on cultured Xenopus muscle cells: electrophoresis, diffusion, and aggregation.** *J Cell Biol* 1988, **107**:1397-1408

16. Stollberg J, Fraser SE: **Acetylcholine receptor clustering is triggered by a change in the density of a nonreceptor molecule.** *J Cell Biol* 1990, **111**:2029-2039
17. Noh N, Sabrina F, Stollberg J: **Development of an Acetylcholine Receptor Aggregate in an Electric Field.** *In: John A. Burns School of Medicine Symposium; University of Hawaii* 1994
18. Kunkel DD, Stollberg J: **Ultrastructural Organization of Electric-Field Induced Acetylcholine Receptor Aggregates.** *In: Neurosci Absts* 1999
19. Baker LP, Chen Q, Peng HB: **Induction of acetylcholine receptor clustering by native polystyrene beads. Implication of an endogenous muscle-derived signalling system.** *J Cell Sci* 1992, **102 (Pt 3)**:543-555
20. Peng HB, Cheng P-C, Luther PW: **Formation of ACh receptor clusters induced by positively charged latex beads.** *Nature* 1981, **292**:831-834
21. Bridgman PC, Nakajima Y: **Distribution of Filipin-Sterol Complexes on Cultured Muscle Cells: Cell-Sustratum Contact Areas Associated with Acetylcholine Receptor Clusters.** *J Cell Biol* 1983, **96**:363-372
22. Bloch RJ, Geiger B: **The localization of acetylcholine receptor clusters in areas of cell-substrate contact in cultures of rat myotubes.** *Cell* 1980, **21**:25-35
23. Mook-Jung I, Gordon H: **Acetylcholine receptor clustering in C2 muscle cells requires chondroitin sulfate.** *J Neurobiol* 1995, **28**:482-492
24. Grow WA, Ferns M, Gordon H: **Agrin-independent activation of the agrin signal transduction pathway.** *J Neurobiol* 1999, **40**:356-365
25. Grow WA, Ferns M, Gordon H: **A mechanism for acetylcholine receptor clustering distinct from agrin signaling.** *Dev Neurosci* 1999, **21**:436-443
26. Grow WA, Gordon H: **Sialic acid inhibits agrin signaling in C2 myotubes.** *Cell Tissue Res* 2000, **299**:273-279
27. Gautam M, Noakes PG, Moscoso L, Rupp F, Scheller RH, Merlie JP, Sanes JR: **Defective Neuromuscular Synaptogenesis in Agrin-Deficient Mutant Mice.** *Cell* 1996, **85**:525-535
28. McMahan UJ: **The agrin hypothesis.** *Cold Spring Harbour Symp Quant Biol* 1990, **55**:407-418
29. Montanaro F, Gee S, Jacobson C, Lindenbaum M, Froehner S, Carbonetto S: **Laminin and alpha-dystroglycan mediate acetylcholine receptor aggregation via a MuSK-independent pathway.** *J Neurosci* 1998, **18**:1250-1260
30. Sugiyama JE, Glass DJ, Yancopoulos GD, Hall ZW: **Laminin-induced acetylcholine receptor clustering: an alternative pathway.** *J Cell Biol* 1997, **139**:181-191
31. Cohen M, Jacobson C, Yurchenco P, Morris G, Carbonetto S: **Laminin-induced clustering of dystroglycan on embryonic muscle cells: comparison with agrin-induced clustering.** *J Cell Biol* 1997, **136**:1047-1058
32. Kunkel DD, Stollberg J: **Ultrastructural Organization of Developing Acetylcholine Receptor Aggregates.** *In: Neurosci Absts* 1996535
33. Kunkel DD, Stollberg J: **Structural Organization of Developing Acetylcholine Receptor Aggregates.** *J Neurobiol* 1997, **32**:613-626
34. Stollberg J, Kunkel DD: **Quantitative Assessment of Aggregate Structure.** *Comments Mol. Cell. Biophys* 2000, **10**:25-52
35. Sabrina F, Stollberg J: **Common Molecular Mechanisms in Field- and Agrin-Induced Acetylcholine Receptor Clustering.** *Cell Molec Neurobiol* 1997, **17**:207-225
36. Lee L, Kunkel DD, Stollberg J: **Differences in number, size, and characteristic spacing of acetylcholine receptor aggregates induced by agrin and laminin-1.**
37. Sabrina F, Stollberg J: **Electric Fields and Agrin Induce Acetylcholine Receptor Clustering via Common Molecular Mechanisms.** *In: Keystone Symposia. Synapse Formation and Function: The neuromuscular junction and the central nervous system II;* 1995
38. Burkin DJ, Kim JE, Gu M, Kaufman SJ: **Laminin and alpha7beta1 integrin regulate agrin-induced clustering of acetylcholine receptors.** *J Cell Sci* 2000, **113**:2877-2886

Appendix

Software identification of gold particle locations

Several different approaches were tested for identification of particle locations in the SEM images. The nature of the problem can be seen in Figure 9A and 9B, which illustrate the difficulty of simply applying a threshold to identify particle locations. The best solution, which works quite well, was found by averaging more than 600 particle images, located by eye, and using this as the kernel for convolution of the SEM image via Fourier transformation. Figure 9C illustrates the result of this convolution, which greatly reduces the noise and intensity ramp seen in B. Finally, the particle locations were defined as the center of mass of contiguous pixel elements above threshold and made up of more than 50 members (Figure 9D). This procedure was tested against small numbers of hand mark particles and found to produced statistically indistinguishable results. In larger applications we expect that it will be more reliable (no inadvertent "double clicks" which have had to be filtered out in software), and more accurate (location of the particle center is not limited to the spatial resolution of the eye or mouse over the SEM image).

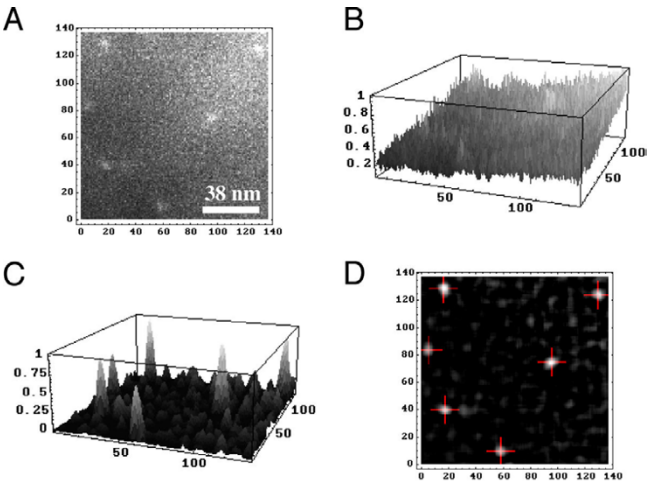

Figure 9
Software determination of gold particle locations. A, enlarged image of raw bitmap showing 6 gold particles. B, 3-Dimensional plot of A illustrates the difficulty in threshold detection of particles. C, the original bitmap convolved with a kernel comprised of the average of 662 gold particles; compare to B with respect to enhancement of gold particle signal and reduction in noise and intensity drift. D, software determination of gold particle locations, based on the center of mass of supra-threshold clusters of pixels. All spatial axes are in units of pixels, coincidentally similar in this instance to the dimensions in nanometers (see calibration in A).

Statistical Analysis

The analysis of nearest neighbor distances involves a serious statistical problem: an individual distance may or may not be statistically independent of the other distances. For any group of three particles, at least two of the three nearest neighbor distances associated with them will be the same. Because of this inherent feature of the analysis, the data are in a sense over-sampled (n is overstated) and the variance is underestimated. This leads for example to the frequent rejection of statistical similarity even in different runs of a simulation known to arise from the same distribution process; the random differences are found to be statistically significant at a frequency much greater than 5% when applying a $p < 0.05$ cutoff.

To compensate for these anomalies the experimental (and simulation) data, were "reduced" prior to statistical comparisons. Nearest neighbor distance distributions were filtered such that pairs of identical distances corresponding to a pair of points were replaced with a single nearest neighbor distance. This brings up another issue: the distribution form for (unreduced) nearest neighbor distances for a random distribution is known analytically (Materials and methods) while that for a reduced data set is at present unknown. We have determined that 1) under some conditions at least the two distributions can be significantly different, but 2) in terms of the actual data analyzed here the differences appear to be quite small (Figure 10). Accordingly we have presented the graphical data in unreduced form (for visual comparison to known distributions) but perform the statistical comparisons on reduced data sets.

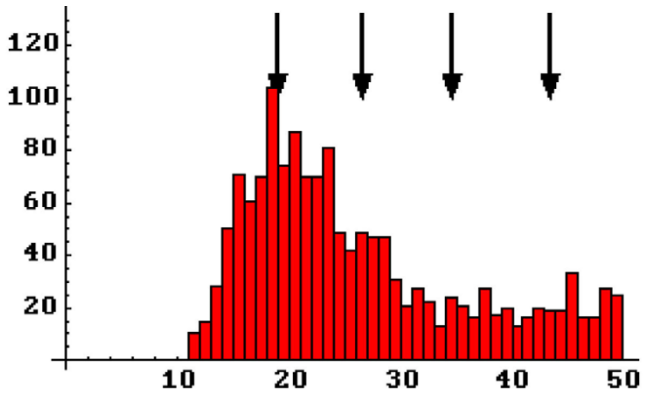

Figure 10
Frequency histogram of reduced nearest neighbor distances in laminin-1 stimulated cells. Although the number of observations has been reduced (n = 1468 vs. 2581 unreduced) the form of the distribution is clearly very similar to that of the unreduced data (compare to Figure 3A).